ACS central science

Research Article

Cite This: ACS Cent. Sci. 2018, 4, 1315−1325

http://pubs.acs.org/journal/acscii

The Impact of Nonequilibrium Conditions in Lung Surfactant: Structure and Composition Gradients in Multilamellar Films

Jenny Marie Andersson,[†,‡] Kevin Roger,*[,‡] Marcus Larsson,[§] and Emma Sparr[†]

[†]Physical Chemistry, Lund University, Lund SE-221 00, Sweden

[‡]Laboratoire de Génie Chimique, Université de Toulouse, CNRS, Institut National Polytechnique de Toulouse, Université Paul Sabatier, Toulouse 31330, France

[§]Department of Pediatrics/Neonatology, Medical Faculty, Lund University, Lund SE-221 00, Sweden

Supporting Information

ABSTRACT: The lipid−protein mixture that covers the lung alveoli, lung surfactant, ensures mechanical robustness and controls gas transport during breathing. Lung surfactant is located at an interface between water-rich tissue and humid, but not fully saturated, air. The resulting humidity difference places the lung surfactant film out of thermodynamic equilibrium, which triggers the buildup of a water gradient. Here, we present a millifluidic method to assemble multilamellar interfacial films from vesicular dispersions of a clinical lung surfactant extract used in replacement therapy. Using small-angle X-ray scattering, infrared, Raman, and optical microscopies, we show that the interfacial film consists of several coexisting lamellar phases displaying a substantial variation in water swelling. This complex phase behavior contrasts to observations made under equilibrium conditions. We demonstrate that this disparity stems from additional lipid and protein gradients originating from differences in their transport properties. Supplementing the extract with cholesterol, to levels similar to the endogenous lung surfactant, dispels this complexity. We observed a homogeneous multilayer structure consisting of a single lamellar phase exhibiting negligible variations in swelling in the water gradient. Our results demonstrate the necessity of considering nonequilibrium thermodynamic conditions to study the structure of lung surfactant multilayer films, which is not accessible in bulk or monolayer studies. Our reconstitution methodology also opens avenues for lung surfactant pharmaceuticals and the understanding of composition, structure, and property relationships at biological air−liquid interfaces.

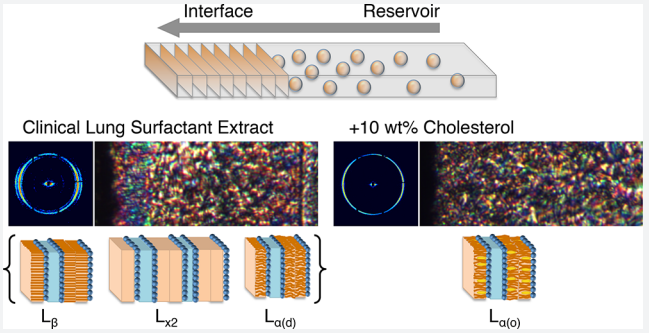

INTRODUCTION

Life for airborne species relies on breathing, a gas exchange process consisting of oxygen uptake and carbon dioxide release. Lungs are the functional organs of breathing and display a large interfacial area between air and water-rich tissue. The bronchoalveolar lung of mammals adopts a treelike structure, with millions of respiratory exchange units termed alveoli.[1] These alveoli are covered with a lipid−protein mixture that is commonly referred to as lung surfactant. Deficiency of the lung surfactant can lead to respiratory distress syndromes. The neonatal respiratory distress syndrome occurs in prematurely born infants, when the lung surfactant is not yet fully developed or completely lacking. This causes alveolar collapse, and it may be lethal if left untreated.[2,3]

Surfactant replacement therapy has revolutionized the care of extreme preterm infants. The common treatment involves an intratracheal administration of an external lung surfactant source.[4] For this therapy, animal-derived surfactants are considered superior over synthetic ones.[5,6] Even though the surfactant replacement therapy has dramatically increased the survival rate,[7] late-effect diseases such as bronchopulmonary dysplasia remain a complication for a high number of extreme preterm births.[8−10] Furthermore, there is no effective corresponding treatment for the adult respiratory distress syndrome, which inflicts high mortality rates of 35−50%.[11,12]

The endogenous lung surfactant is a multicomponent system consisting of approximately 80 wt % phospholipids, with a majority of the disaturated dipalmitoylphosphatidylcholine (DPPC) but also ∼10−15 wt % charged lipids. It also contains ∼7−10 wt % cholesterol and ∼7−10 wt % proteins (SP-A, SP-B, SP-C, SP-D).[13,14] In the present study, we have used samples composed of the clinical surfactant replacement Curosurf, which is commonly used in surfactant replacement therapies in clinics throughout the world.[6] Curosurf is composed of water-insoluble lipids and is therefore formulated as a multilamellar vesicle dispersion in water. Curosurf has like other clinical extracts a much lower cholesterol (0−1 wt %)[15] and protein content (no SP-A or SP-D, less SP-B and SP-C)[14] than the endogenous lung surfactant. On the contrary, the phospholipid composition appears rather unaffected by the extraction.[14]

Received: June 8, 2018
Published: September 24, 2018

DOI: 10.1021/acscentsci.8b00362
ACS Cent. Sci. 2018, 4, 1315−1325

The lung surfactant film mesostructure is a key characteristic of this biomaterial, since it determines both mechanical and transport properties. Two main molecular arrangements for the lung surfactant film have been proposed: (i) a lipid monolayer adsorbed at the air−liquid interface,[2,16−20] and (ii) a thicker multilayer composed of several connected lipid bilayers, such as the tubular myelin arrangement or multilamellar aggregates.[21−24] The structural distinction between a monolayer and a thicker multilayer is crucial when describing the functional properties of lung surfactant. Indeed, a coherent multilayer structure provides a reservoir of material, which decreases the free energy cost of area expansions occurring during a breathing cycle.[25] The multilayer arrangement will also influence diffusional transport of small molecules across the interfacial layer.[26]

The lung surfactant film is situated in nonequilibrium conditions, which are both mechanical, because of the expansion and contraction in the breathing cycle, and thermodynamic, because of the water chemical potential difference between tissue and air. In the present paper, we specifically investigate the interplay between thermodynamic nonequilibrium conditions, the buildup of concentration gradients, and the formation of a multilamellar film at the air−liquid interface.

The lung surfactant layer is a lipid-rich multilayer film situated in between the water-rich tissue and a vapor phase, similarly to the stratum corneum covering our skin or the lipid tear film protecting our eyes.[27,28] If the lung was a closed equilibrium system, the vapor phase relative humidity in the lung would be around 99.6% relative humidity (RH), which corresponds to physiological osmotic pressure at 37 °C. Estimations of moisture patterns in the airways during tidal breathing have shown on a clear RH gradient in the respiratory system where the humidity approaches full saturation in the terminal airspaces.[29] However, there are uncertainties regarding the exact RH values in terminal airspaces due to inherent methodological difficulties in determining RH at very high humidities using, for example, hygrometric techniques. Dew point methods suggest that the alveolar air is not fully saturated.[30] Furthermore, at forced respiration, or in physiological extreme conditions when breathing cold or dry air, the RH gradient will be amplified. The importance of nonsaturated air in the lung was previously also underlined when studying free-forming lung surfactant films at air−liquid interfaces.[31,32]

When the lung surfactant layer is exposed to air with humidity below 99.6%, a water gradient will build up across the layer. Even though this humidity drop is very small, it will have a large impact at the molecular level. For instance, a 1% decrease in relative humidity is equivalent to a 1.3 MPa change in osmotic pressure, which corresponds to changing the saline concentration from 150 to 425 mM.[33] From a thermodynamic standpoint, the lung surfactant film is thus placed in between two boundaries of different water chemical potential. This nonequilibrium condition translates into a free energy field extending through the lung surfactant film, which triggers fluxes of matter and thus the buildup of composition gradients throughout the interfacial multilayer structure. The variation in water chemical potential will influence lipid self-assembly in terms of phase behavior and water swelling, as previously demonstrated for simple phospholipid systems.[34,35]

In this work, we use a recently designed millifluidic setup to monitor composition and structure gradients arising in an evaporation-induced free energy field[36] (Figure 1). We show that this setup enables the concentration and fusion of lipid vesicles, and thus the spontaneous buildup of a multilamellar film at the air−liquid interface, and we characterize both composition and structure gradients within these films. We reach high spatial resolution using small-angle X-ray scattering with micrometric beam size to determine the variations in mesostructure along the composition gradients, which are in turn characterized through infrared and Raman microscopy. We also evaluate the impact of cholesterol on the structure of lung surfactant multilamellar films reconstructed from Curosurf. Indeed, the cholesterol content in endogenous lung surfactant has previously been shown to have large consequences for self-assembly in bulk and monolayer conditions,[37−39] and it has been linked to the *in vivo* performance.[40] Finally, our setup makes it possible to make an evaluation of the deposition process of lung surfactant at the air−liquid interface, in a situation that is similar to the clinical one.

RESULTS AND DISCUSSION

Film Formation at the Air−Liquid Interface. To quantitatively monitor self-assembly structure and composition gradients in lung surfactant multilamellar films, we used a recently designed millifluidic setup (Figure 1), as first described by Roger et al.[36] The cell consists of a borosilicate capillary with a rectangular cross-section 0.1 × 1 mm, which connects on one end to a large reservoir filled up with an aqueous solution, while its other end is exposed to an air flux of controlled relative humidity (RH). In this setup, transport occurs through unidirectional advection and diffusion along the capillary axis. Furthermore, boundary conditions at both ends are controlled and kept constant. Self-assembly structures at different positions in the water gradient were characterized using high-resolution small-angle X-ray scattering. In addition, the gradient in water content was obtained from infrared microscopy experiments, and the dynamics of film formation

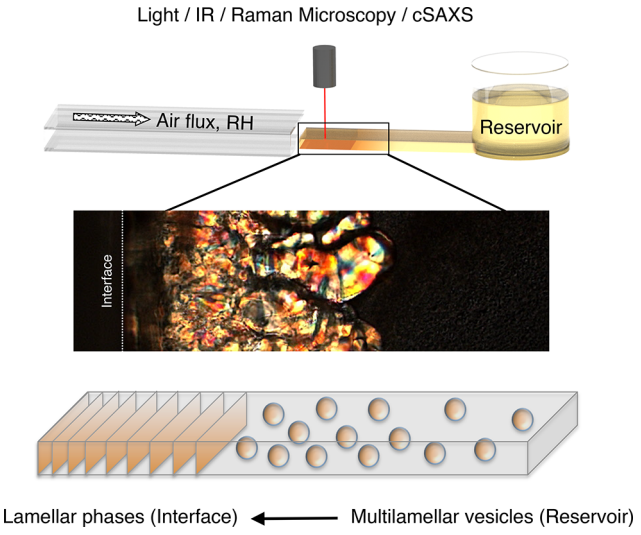

Figure 1. Schematic view of the millifluidic setup, which consists of a rectangular capillary connected on one end to a reservoir of the Curosurf vesicular dispersion and exposed on its other end to an air flux of controlled relative humidity (RH). Water evaporation leads to the buildup of a multilamellar film through multilamellar vesicle fusion, which is birefringent under crossed polarizer observation.

DOI: 10.1021/acscentsci.8b00362
ACS Cent. Sci. 2018, 4, 1315−1325

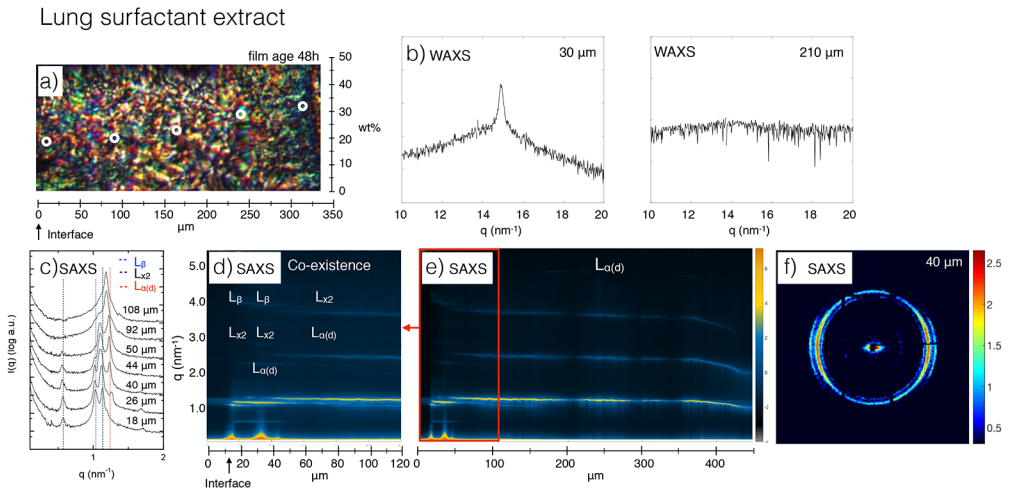

Figure 2. Lung surfactant film assembled from a lung surfactant extract dispersion, Curosurf, at 97% RH, 37 °C, and 48 h evaporation time. (a) Microscopy image taken under crossed polarizers. Overlaid white dots quantify the water gradient across the film, which is determined by infrared microscopy. (b) Wide-angle X-ray scattering (WAXS) 1D spectra at two different positions making evident solid lipid chains in the vicinity of the air−liquid interface. (c) Small-angle X-ray scattering (SAXS) 1D spectra at different positions, displaying the three lamellar phases' coexistence, which have been assigned to a double-spaced lamellar phase ($L_{\times 2}$), a lamellar gel phase (L_{β}), and a lamellar liquid-disordered crystalline phase ($L_{\alpha(d)}$). (d, e) SAXS maps of the scattering vector magnitude, q, versus the distance from the air−liquid interface. Map d is a zoom-in of map e and displays the three lamellar phases' coexistence in the vicinity of the air−liquid interface (about 20% of the total film thickness). Map e shows that this phase coexistence progressively disappears at larger water contents when moving further away from the air−liquid interface. (f) Two-dimensional SAXS pattern displaying a preferential orientation of the different structures along the same direction, which demonstrates that structures are unidimensional.

was studied using polarized optical microscopy. For all lung surfactant extracts investigated, a multilamellar structure spontaneously builds up at the air−liquid interface through the concentration and fusion of the dilute aqueous vesicle dispersion. Film formation was observed through an optical microscope using a crossed polarizer/analyzer setup. Depending on the system, one or several birefringent phases were visualized at the interface (example in Figure 1).

The millifluidic setup operates dynamically so that a steady-state is never reached. Gradients thus propagate in the capillary over time. Nevertheless, we have demonstrated that this propagation follows a scaling law and that gradients are a function of a single variable coupling time and space.[41] In this experimental setup, absolute values of time and thicknesses thus bear no significance. Gradients can be rescaled to invariant profiles that only depend on the system considered and the boundary conditions. The scaling behavior brings experimental opportunities since the study of thin interfacial structures, such as the lung surfactant multilamellar film, can be scaled up to thicker films for which a much higher spatial resolution can be attained with the experimental methods at hand. The measured profiles in structure and composition can then be rescaled to the thickness of interest. Therefore, even though we typically grew films to a few hundred microns in the present experiments, the different composition and structure gradients can be directly rescaled to the thinner thicknesses expected for *in vivo* lung surfactant films. Indeed, while the exact *in vivo* film thickness is difficult to measure, it is at least of 0.2 μm.[42,43] This corresponds to a few dozen bilayers, which is sufficiently large to spread the gradients made evident in this work. Similarly, the vesicle concentration in the dispersion only plays a role on the film growth rate, since it directly relates to the amount of lipids transported toward the growing film, but not on the different gradient profiles.

Interfacial Self-Assembly in Lung Surfactant Multilamellar Films. Self-assembly structures at different positions within the interfacial multilamellar lung surfactant films were monitored using SAXS and WAXS. We used small beam sizes of 1.4 × 5 μm, with the smallest dimension taken along the capillary axis to maximize the spatial resolution of the gradient profile. In all systems investigated, we observed one or more lamellar phases, appearing as evenly spaced Bragg reflections in the SAXS spectra (Figures 2 and 3). No other types of self-assembly structures were detected. The repeating unidimensional units of lamellar phases are typically bilayers with fluid or solid chains. The presence of solid acyl chains can be distinguished from the WAXS spectra, where a prominent 4.1 Å reflection corresponds to a gel-state bilayer with hexagonally packed acyl chains.[44]

Figure 2 displays the scattering and microscopy data obtained for the clinical lung surfactant extract, using a relative humidity of 97% RH. The SAXS microscopy experiments yield structure maps (Figure 2) obtained from the individual SAXS spectra (examples of 1D spectra and 2D patterns are shown together with the structure maps in Figure 2), where the x axis corresponds to the position in the capillary, the y axis gives the q values, and the color scale corresponds to the logarithm of the scattered intensity.

In the samples with low cholesterol content, a single phase is observed over 80% of the film. Two-dimensional SAXS patterns indicate that this phase is unidimensional; 1D SAXS spectra show evenly spaced diffraction peaks, and WAXS spectra indicate liquid hydrocarbon chains. These observations are characteristic of the lamellar liquid-disordered phase, $L_{\alpha(d)}$. Moving closer to the air−liquid interface, which corresponds to the remaining 20% of the film, this $L_{\alpha(d)}$ first coexists with other phases, and ultimately disappears. WAXS spectra indicate the presence of crystalline hydrocarbon chains in the outer region of the multilayer film (Figure 2b), while SAXS spectra

DOI: 10.1021/acscentsci.8b00362
ACS Cent. Sci. 2018, 4, 1315−1325

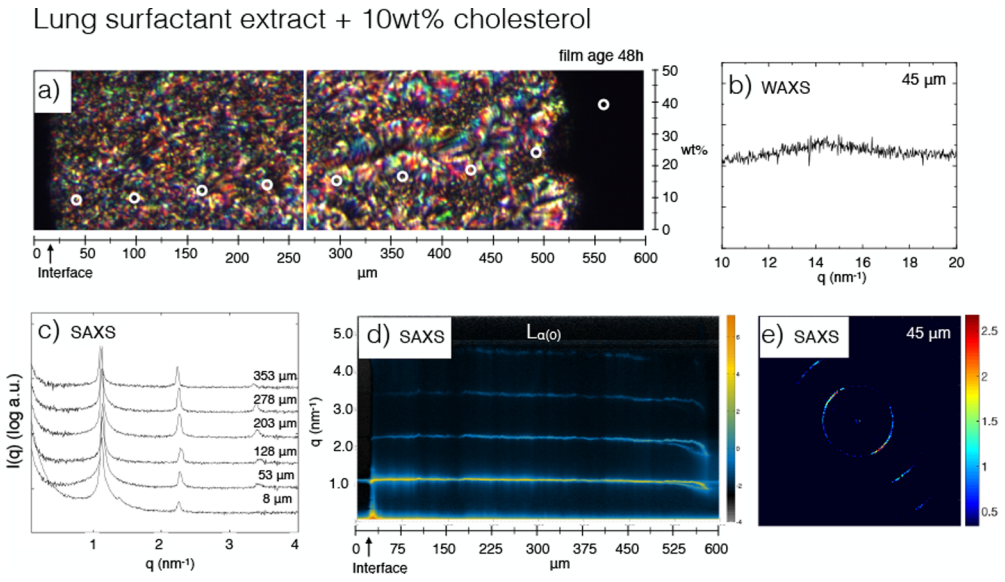

Figure 3. Lung surfactant film assembled from a 10 wt % cholesterol-supplemented lung surfactant extract dispersion, Curosurf, at 97% RH, 37 °C, and 48 h evaporation time. (a) Microscopy image taken under crossed polarizers. Overlaid white dots quantify the water gradient across the film, which is determined by infrared microscopy. (b) Wide-angle X-ray scattering (WAXS) 1D spectrum showing liquid lipid chains. (c) Small-angle X-ray scattering (SAXS) 1D spectra at different positions, displaying a single lamellar phase throughout the whole film. (d) SAXS maps of the scattering vector magnitude, q, versus the distance from the air−liquid interface. A single lamellar phase with limited swelling is observed. (e) Two-dimensional SAXS pattern displaying a preferential orientation of the lamellar structure, but continuously rotating from one position to another.

indicate two different lamellar spacings. Two-dimensional patterns show that both structures are aligned along a single direction and are thus unidimensional. One of these two structures displays all the characteristics of a planar lamellar gel phase (L_β). The other structure presents a weak first order peak at a much lower q value than for the two other lamellar structures. The measured d spacing of this third phase is indeed close to twice the average spacing of $L_{\alpha(d)}$ and L_β phases. One possibility would be to assign this structure to the two-dimensional phase, with the first peak corresponding to the ripple spacing (Figure S1). Indeed, such ripple phases can be observed in between the planar gel phase and the $L_{\alpha(d)}$ phases.[45] However, as stated above, the 2D patterns indicate that both first and second peaks are aligned in the same direction, which is not consistent with the ripple phase structure.

The scattering pattern (Figure S2) corresponding to the peak at low q value is similar to that of the L_γ phase presented by Luzzati and co-workers in the 1970s,[46,47] in their phase diagram studies of mitochondrial lipids. They observed the characteristic reflection pattern of a lamellar phase but with a very weak or absent first order peak, and with a spacing that was double that of a usual lipid lamellar phase. From this pattern, a lamellar phase with four monolayers in the unit cell was proposed. Interestingly, similar SAXS patterns have later also been reported for natural lung surfactant extracts with similarities to Curosurf.[48−50] A similar scattering pattern was recently also reported for mixed phospholipid vesicles in the presence of peptides.[51] The formation mechanism of such an original lamellar structure likely originates from protein/lamellae interactions, for instance, through anchoring or bridging. Different lipid chain arrangements have been proposed for the observed double lamellar phases, but we have no experimental evidence to select one over the others. Furthermore, we have not observed the double spacing lamellar structure for equilibrium bulk conditions corresponding to the global lipid and protein composition of Curosurf dispersions (Figures S4 and S5), which precludes a formal identification of this structure as an equilibrium one. Therefore, we prefer to use the notation $L_{\times 2}$ to make a distinction between the observed structure and the L_γ equilibrium phase and its different possible molecular arrangements.

Overall, we observe from the bulk to the air−liquid interface the expected dehydration-induced transition between lamellar structures with fluid and solid acyl chains in the lung surfactant extract. This dehydration transition is analogous to the temperature-induced melting transition, and has previously been investigated for simple model systems relevant to the lung surfactant[34,45] and for a lung surfactant extract under bulk conditions.[52] However, in the interfacial film, we observe a different phase behavior, which is the formation of the $L_{\times 2}$ structure. The $L_{\times 2}$ structure is observed over a large region in the multilamellar film, corresponding to a significant range in water activity. On the contrary, in the bulk systems, the scattering data does not display any signs of the $L_{\times 2}$ structure in the relevant range of RH (75% and 97% RH) and temperature (30−40 °C, Figures S4 and S5, Supporting Information). Furthermore, lamellar spacing for both $L_{\alpha(d)}$ and L_β phases significantly differs between the bulk and the capillary experiments, as shown by comparing Figures S4 and S5 and Table S1 with Figure 2.

Nonequilibrium Transport Effects in Multicomponent Systems. We now turn toward an explanation of why nonequilibrium conditions in the capillary setup have such a large impact on the mesostructure of the interfacial multilayer film. Indeed, our previous study on simpler binary surfactant systems strongly supported local thermodynamic equilibrium and did not display any such nonequilibrium effects.[36] It is likely that for a multicomponent system, such as lung surfactant, more than one composition gradient builds up in the interfacial multilayer film, as previously predicted for

DOI: 10.1021/acscentsci.8b00362
ACS Cent. Sci. 2018, 4, 1315−1325

ternary systems.[53] In such situations, the lipid distribution within the multilayer film will not be uniform, and the outer layer of the film can then be enriched in certain lipid components. This nonuniform distribution of lipid components can be explained by differences in diffusional properties of the various components within the interfacial mesoscopic structures.[53,54] Comparisons with equilibrium bulk studies for similar systems and conditions[55−58] make it clear that small changes in composition can have a large impact on self-assembly structures. This implies that a minor shift in the balance between different lipid components in the interfacial multilayer film can lead to clear deviations from the bulk self-assembly structures. Similarly, proteins may also distribute heterogeneously within the film, which could also have structural consequences. In our particular case, the $L_{\times 2}$ structure could arise from local composition changes compared to the bulk samples. In principle, the observed structure could thus be obtained at equilibrium but for different bulk compositions.

First, to investigate the existence of a lipid gradient superimposed on the water gradient, we performed Raman confocal microscopy (Figures S6 and S7). We indeed observed that the ratio[59] between the 1655 cm^{-1} peak, corresponding to the C═C double bond bend, and the 1444 cm^{-1} peak, corresponding to CH_2 scissors and CH_3 degenerate deformation, decreased within the multilayer film toward the air−liquid interface. The amount of unsaturated lipids was systematically lower in the region where the $L_{\times 2}$ structure was observed. This lipid gradient arises within the forming film since the vesicle compositions remained constant in the bulk dispersion up to their fusion. In the multicomponent lung surfactant system, the gradient in lipid composition may have functional consequences if the outer layer that is exposed to the oxygen-rich vapor phase is enriched in saturated lipids. Such accumulation of saturated lipids, which are here mainly DPPC,[13,14] in the vicinity of the air−liquid interface is also consistent with the disappearance of the $L_{\alpha(d)}$ phase in the outer layer of the multilayer film, while this phase is observed in the bulk samples of Curosurf for all corresponding humidity and temperature conditions (Figures S4 and S5). The induced gradient in the ratio between saturated and unsaturated lipids could also explain the smaller lamellar swelling observed in the outer layer of the multilayer films as compared to the bulk Curosurf samples. Indeed, the majority of the anionic phospholipids in lung surfactant extracts is unsaturated[37,60] and likely depleted from the vicinity of the air−liquid interface. A reduction of charged lipids will reduce the electrostatic repulsion and thereby reduce the swelling of the lamellar phase.

Second, the Raman spectra obtained for lung surfactant multilayer films displayed a large fluorescence background signal, which we believe is due to the presence of proteins in the Curosurf mixture. The intensity of this background fluorescence signal systematically increases by an order of magnitude when going from the bulk vesicle dispersion toward the outer layer of the multilayer film in the capillary (Figure S8). This observation suggests that the proteins present in the Curosurf sample, SP-B and SP-C, are also unevenly distributed in the multilayer film. Indeed, these proteins accumulate close to the air−liquid interface. Such a protein gradient may explain the formation of the $L_{\times 2}$ structure similarly to what has been found for other lipid−protein systems,[51] including previous studies of natural lung surfactant.[48] Indeed, SP-B may bridge two opposite monolayers while SP-C may anchor one bilayer to another monolayer. Their accumulation at the air−liquid interface would thus favor the formation of a double bilayer lamellar cell.

Cholesterol and Calcium Ion Effects on Lung Surfactant Films. All lung surfactant extracts used in clinical treatments of neonatal respiratory distress syndrome (RDS), including Curosurf that we used in this study, have a significantly lower cholesterol content compared to the endogenous lung surfactant.[13] We verified the cholesterol content of our Curosurf sample and found it was under the detection limit of our spectroscopic method (⩽0.1 mmol/L). The lipid and protein content of Curosurf has been determined by several groups previously.[14,15,61] Curosurf contains neither SP-A nor SP-D[61,62] and lower amounts of SP-B and SP-C than the endogenous lung surfactant.[14]

A strong effect of cholesterol on the phase behavior of lung surfactant extracts has previously been shown in bulk samples.[37,39,63] The addition of 10 wt % cholesterol to a clinical grade extract induced a transition from coexisting lamellar gel and liquid crystalline lamellar phases to one liquid lamellar phase with a higher order of the acyl chains. We thus investigated the impact of cholesterol addition on the lung multilayer films in the capillary setup. In the cholesterol-containing systems, at both RH investigated, a single lamellar phase was observed throughout the whole film by SAXS. No sign of crystalline packing of acyl chains was detected by WAXS (Figure 3b and Figures S9 and S10 in the Supporting Information).

Multilamellar films reconstituted from lung surfactant extracts were also studied in the presence of divalent Ca^{+2} ions with similar results as shown for the samples with no Ca^{+2} ions. This implies that the multilayer self-assembly structures in the lung surfactant extracts are not related to ion-specific effects. However, the potential role of calcium ions in lung surfactant may be absent in Curosurf because of the absence of hydrophilic proteins SP-A and SP-D. The data from the

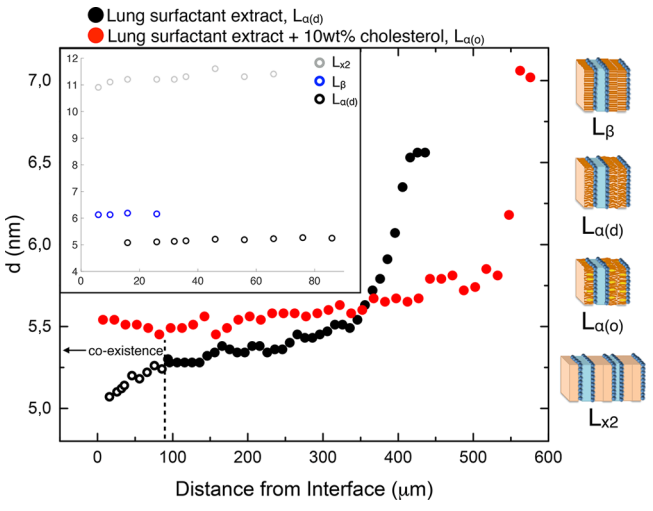

Figure 4. Lamellar repeat distance, d, for the L_α phases in films formed at 97% RH from (black ●) lung surfactant extract ($L_{\alpha(d)}$) and (red ●) lung surfactant extract +10 wt % cholesterol ($L_{\alpha(o)}$). The region where the $L_{\alpha(d)}$ phase coexists with $L_{\times 2}$ and L_β phases in the clinical extract is separated with a dotted line. Repeat distances of the (blue ○) L_β phase and (gray ○) $L_{\times 2}$ phase are shown in insert together with the repeat distances for the (black ○) $L_{\alpha(d)}$ phase.

DOI: 10.1021/acscentsci.8b00362
ACS Cent. Sci. 2018, 4, 1315−1325

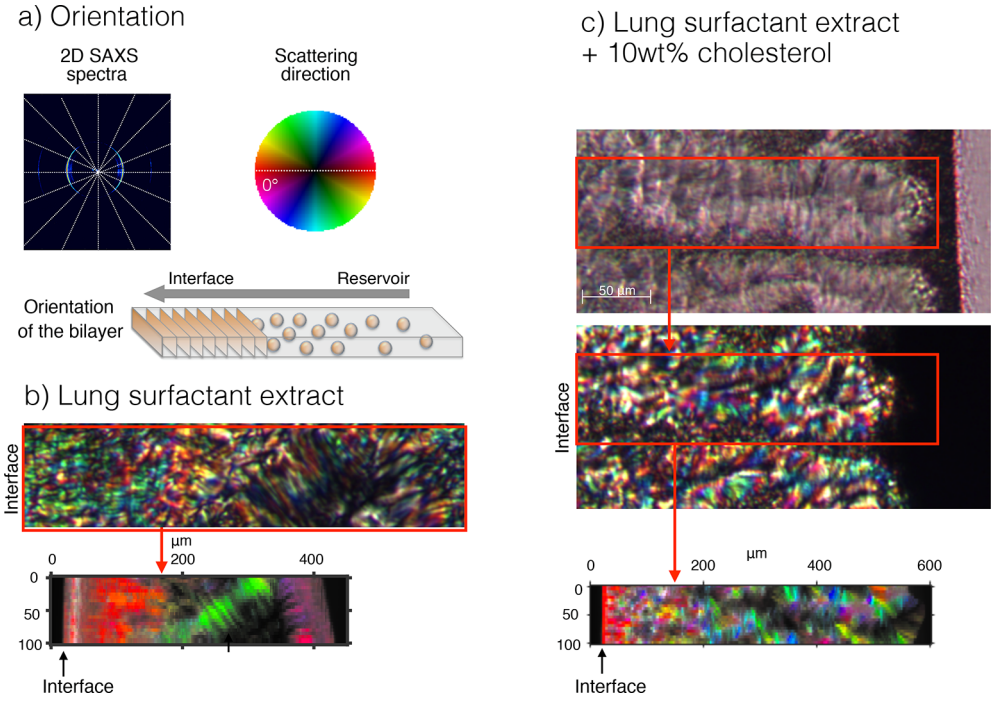

Figure 5. (a) Explanation of the orientation maps. The orientation is derived from the 2D spectra of the SAXS measurements which are divided into 16 slices. The intensity in each slice is analyzed to determine the preferential orientation. The color code indicates preferential bilayer orientation, with red corresponding to scattering at 0° and thus to bilayers oriented parallel to the air−liquid interface. The color intensity indicates how strong the alignment is, with black indicating no alignment. (b) Bilayer orientation map for the L_α phase of a lung surfactant film assembled from the clinical extract dispersion, Curosurf, at 97% RH. Lamellae remain parallel to the air−liquid interface in a third of the film. (c) Bilayer orientation map for the L_α phase of a lung surfactant film assembled from the 10 wt % cholesterol-supplemented clinical extract dispersion, Curosurf, at 97% RH. Lamellae remain parallel to the air−liquid interface in a third of the film. The long-range alignment is lost, with lamellae continuously rotating within the film.

samples with Ca^{+2} ions is shown in the Supporting Information (Figures S11 and S12).

Swelling Profiles in Lung Surfactant Films with and without Cholesterol. To quantify the variation in water content in the interfacial multilayer, we performed near-infrared microscopy experiments at a spatial resolution of 25 μm. A broad band at 4800−5300 cm^{-1} in the spectra corresponds to the OH bend−stretch combination band of water. The integral of this peak thus quantifies the amount of water in the sample.[64] We mapped out the capillary by taking a spectrum every 20 μm, which allows us to calculate the amount of water for each position. The water gradient build-up in the capillary was observed over time. The water concentration measurements at different positions in the capillary are superimposed on the optical microscopy images in Figure 2a and Figure 3a, showing a close to linear variation in water content across the multilayer. This behavior closely resembles observations made for simpler model systems.[36] In the lung surfactant samples with multiple coexisting phases there is a gradual change in water content across the phase boundary region, which is expected for systems where there is a gradual redistribution between the different lamellar phases. The water content in the immediate vicinity of the air−liquid interface displays a dependence with the outside humidity. Multilamellar films exposed to air with 97% RH exhibit a less steep water gradient between interface and the bulk solution compared to the film formed in dryer conditions (Figures S13−S16, Supporting Information). Finally, there is an abrupt change in water content at the boundary between the lamellar interfacial film and the aqueous dispersions of multilamellar vesicles.

To obtain a more detailed characterization of the swelling profile, we quantified the lamellar repeat distances as a function of position in interfacial layer based on the SAXS experiments. Figure 4 shows the variation in the lamellar repeat distance (d) of the L_α phases as a function of the position in the interfacial multilamellar film at 97% RH. For the lung surfactant system with physiological levels of cholesterol, the single $L_{\alpha(o)}$ phase show a very smooth and shallow swelling profile within the whole film at both 97% RH and 75% RH (Figure 4 and Figure S18), implying a close to homogeneous interfacial film even for relatively large water gradients. This is consistent with previous observations showing that the liquid-ordered lamellar phase is rather resilient to changes in water activity.[65] The measured repeat distances of the $L_{\alpha(o)}$ multilamellar structure with cholesterol lie in between those of the L_β and $L_{\alpha(d)}$ phases in the cholesterol-poor sample. For the sample with low cholesterol content, there is a stronger variation in swelling over the interfacial film of the $L_{\alpha(d)}$ phase (Figure 4). The swellings of the different phases in the region of the film where the phases coexist are folded in Figure 4. While the L_β phase hardly swells at all (from 6.12 to 6.15), the $L_{\times 2}$ spacing slightly increases in the film from 10.9 nm at the interface to 11.4 nm where the double lamellar phase disappears. Swelling profiles for samples measured at 75% RH or with Ca^{2+} ions are shown in the Supporting Information, Figures S17−S19.

Overall, films with low cholesterol content displayed not only phase coexistence but also substantial swelling while films with a higher cholesterol content displayed a single phase with

DOI: 10.1021/acscentsci.8b00362
ACS Cent. Sci. 2018, 4, 1315−1325

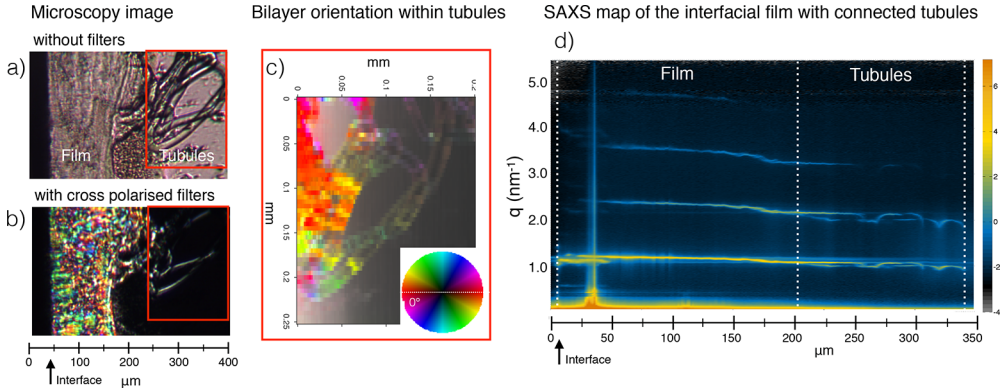

Figure 6. Microscopy images without (a) and with (b) crossed polarizers, showing tubule formation at the film growth front. (c) Orientation map from 2D SAXS patterns show that lamellar domains are weakly oriented along curls in the tubules. (d) SAXS map showing that tubules are made from lamellae directly connected to the film and with similar spacing as within the inner part of the film.

limited swelling. The addition of cholesterol in amounts comparable to the endogenous lung surfactant thus results in a much more homogeneous film than what is obtained with the lung surfactant replacement Curosurf that contains little cholesterol.

Orientation of the Bilayers in the Interfacial Film with and without Cholesterol. The 2D scattering patterns (Figure 2) clearly indicate an alignment of the lamellar phases close to the air−liquid interface. For the lung surfactant extract the majority of the multilayers have bilayers that are oriented parallel to the interface. Alignment maps of the bilayers in the L_α phase of lung surfactant extract and extract +10 wt % cholesterol films formed at 97% RH an explicit bilayer orientation throughout the multilamellar film (Figure 5). Bilayer alignment is extracted from the 2D SAXS spectra (example in Figure 5a) as an oriented structure will give rise to scattering at distinct positions. In Figure 5, orientation maps are color-coded, where red corresponds to bilayers oriented parallel to the interface. The color intensity indicates how strong the alignment is with black indicating the absence of alignment. In the vicinity of the air−liquid interface, bilayers are strongly oriented parallel to the interface. Alignment is progressively lost when approaching the dilute solution in the reservoir. Bilayers are similarly oriented in films formed from clinical lung surfactant extract at 75% RH and/or with Ca^{+2} ions. The corresponding orientation maps are shown in the Supporting Information, Figures S3, S12, and S11. We interpret this alignment as a resulting of epitaxial templating from the lipid monolayer separating liquid from air, which is oriented parallel to the interface. This orientation would propagate throughout the film to minimize defect costs. This is especially noticeable when a gel phase is present, while the orientation changes when only the $L_{\alpha(d)}$ is observed.

In the films built from the cholesterol-supplemented extract, bilayer orientation parallel to the air−liquid interface is only observed close to the edge. In the rest of the multilamellar film, bilayer orientation undergoes a continuous rotation, which yields channels. This loss of orientation in the $L_{\alpha(o)}$ phase compared to both $L_{\alpha(d)}$ and gel phases could relate to the molecular-scale segregation effects that have been suggested in such phases.[66]

Tubule Formation in the Swelling Limit. In this study, multilamellar films are formed from lipids and proteins delivered to the interfacial layer from a bulk solution containing dispersed multilamellar vesicles. During the buildup of the film, lipids are transferred from vesicles to the oriented interfacial layer through fusion processes. It is a recurring observation for all systems investigated that the fusion of vesicles with the interfacial film is associated with the formation of tubular structures (Figure 6) that have similarities to the myelination,[67−70] fingering,[62,71] and tubulation[72−74] phenomena, which have been previously described for other systems. The mesostructure of the tubules was determined by SAXS, showing a lamellar phase with identical repeat distance as the inner fully swollen layer of the multilamellar film but an orientation along the curling of the tubules (Figure 6). Similar tubular structures have also been observed by Parra et al. in other lung surfactant systems placed in micropipettes under pressure. They observed that the presence of a synthetic peptide analog of the surfactant protein SP-B promoted the formation of the tubule structures.[75]

CONCLUSIONS

In this work, we have developed a methodology to assess the effect of both composition and nonequilibrium conditions on the interfacial structure of a lung surfactant clinical extract. Multilayer interfacial structures spontaneously form from the aqueous dispersion of a lung surfactant extract by concentrating a vesicular dispersion in a millifluidic channel. Even at a high relative humidity of 97% in the vapor phase, which is relevant to the physiological conditions, the difference in water chemical potential between the liquid and the gas leads to the buildup of a multilamellar film over time.

For the clinical extract, which contains only trace amounts of cholesterol, the self-assembly structure strongly varies with position in the multilamellar film. In the vicinity of the air−liquid interface, three coexisting lamellar phases are observed, a liquid-disordered lamellar phase ($L_{\alpha(d)}$), a planar gel phase (L_β), and a double lamellar phase ($L_{\times 2}$). Further away from the air−liquid interface, the two lamellar gel phases subside, yielding only the $L_{\alpha(d)}$ phase. Furthermore, a substantial variation in water swelling of the $L_{\alpha(d)}$ phase was observed within the water gradient. The lamellar phases strongly align with lamellae parallel to the interface, notably for the $L_{\alpha(d)}$ phase.

Importantly, bulk characterizations of the Curosurf lung surfactant extract equilibrated at 97% RH yielded only two lamellar phases, the liquid-disordered and the planar gel phase. The double lamellar ($L_{\times 2}$) phase, which is predominant in the vicinity of the air−liquid interface, is thus absent in equilibrium

DOI: 10.1021/acscentsci.8b00362
ACS Cent. Sci. 2018, 4, 1315−1325

bulk conditions. Indeed, thermodynamic nonequilibrium conditions generate fluxes and transport of matter. Since transport properties are molecular-dependent in multicomponent systems, several composition gradients arise. Locally, ratios between different lipids and protein concentration may thus deviate from bulk conditions, which impacts the self-assembly behavior. This disparity between equilibrium and nonequilibrium conditions highlights the relevance of our methodology, in which we perform structural characterizations in relevant nonequilibrium conditions. This generic method also shares some similarities with a deposition process such as the intratracheal administration of lung surfactant. A practical conclusion regarding the clinical porcine extract is its nonrobustness in terms structural diversity, arising in response to the small water gradient.

Adding cholesterol in amounts representative of the endogenous lung surfactant composition completely modified the interfacial film self-assembly structure. Both elements of structural complexity, the triple phase coexistence and large variations in water swelling, vanished upon adding cholesterol. Instead, a much simpler interfacial multilayer is obtained, which consists of a homogeneous liquid-ordered lamellar phase with relatively flat swelling profile in the water gradient. The lung surfactant system is thus an interesting illustration that, in multicomponent systems, structural complexity can decrease upon adding an additional component. This effect of cholesterol to abolish phase transitions and form a uniform lamellar structure over a range of hydration conditions has also been demonstrated in simple phospholipid model systems at varying osmotic pressures.[76] In the inner water-rich layer of the cholesterol-containing multilamellar films, alignment of the lipid bilayers parallel to the interface is lost and replaced by a succession of rotating channels. This demonstrates that not only the microstructure but also the mesostructure is altered upon adding cholesterol to the lung surfactant extract. Overall, our observations highlight the importance of cholesterol on lung surfactant films structure and the importance to consider nonequilibrium effects on the structure and composition of the interfacial film. In the *in vivo* lung surfactant film covering the alveolar interface, the presence of cholesterol may serve to prevent segregation and domain formation, which would have a strong impact on diffusional transport across the layer as well as mechanical and elastic properties during breathing expansion retraction cycles.

MATERIALS AND METHODS

Sample Preparation. Curosurf water dispersions were used for all measurements at concentrations of either 16 or 40 mg/mL. The samples were diluted in aqueous solutions containing either 150 mM NaCl with 0.2 mM EDTA and 0.02 wt % NaN_3 or 138 mM NaCl and 4 mM $CaCl_2$ with 0.02 wt % NaN_3. Small amounts of antibacterial (NaN_3) is used in all samples to prevent contamination by bacterial growth. Control experiments were done without NaN_3, and no detectable difference on the interfacial films was observed. The Curosurf +10 wt % cholesterol samples were prepared by adding cholesterol in chloroform solution to the vial and letting it dry to a thin cholesterol film under a stream of N_2. The Curosurf vesicle dispersion was then added, and the solution was left to equilibrate on a shaking board for 1 week after which no visible cholesterol film was left. Cholesterol in water dispersions does not form self-assembled structures on its own but will be dissolved in the vesicles. All samples, both with and without cholesterol, were sonicated with a CupHorn 70% amplitude 10:5 pulse for 40 min at 40 °C to homogenize the solutions. A water chiller was connected to the CupHorn instrument ensuring a constant temperature during the entire sonication process.

Capillary Cells. Capillary cells are made in-house of borosilicate glass rectangular capillaries (1 × 0.1 mm) attached by a UV-hardening glue (Norland Optical Adhesive, NOA63) to a plastic container holding the bulk. The capillaries were precoated with Curosurf solution and subsequently washed with water prior to final film formation. The humidity was controlled by either storing the capillary cells in closed desiccators at 37 °C containing saturated salt solutions of either NaCl (75% RH) or K_2SO_4 (97% RH) or during measurements by a larger capillary connected to N_2 gas led through 3 consecutive bubblers with saturated salt solutions.

Small-Angle X-ray Scattering. Small-angle X-ray scattering measurements were done at the X12SA (cSAXS) beamline at the Swiss Light Source, Paul Scherrer Institut, Zurich, Switzerland. A monochromatic beam of 11.2 keV and beam size 5 × 1.4 μm was used. Scattering was recorded with a Pilatus 2 M detector separated from the sample by a 2 m evacuated flight tube. Sample cell capillaries were mounted on a two-axis scanning stage coupled to a microscope to be able to follow where measurements were done in the capillary. Exposure time was set to 0.5 s for the majority of the measurements. Temperature was kept during measurements by a copperplate connected to a heated water bath. Humidity was controlled by humidified N_2 gas.

Polarized Light Microscopy. A Zeiss Axioplan microscope was used to acquire images of the lung surfactant films. The capillary cells were positioned between two cross-polarized filters to distinguish between isotropic and birefringent phases. A magnification of 20× was used for all images which were acquired with a color camera and the accompanying Zeiss software. Images were typically sampled every 30 min. The scale of the images was decided by the observation of a ruler of known size. The humidity was kept during the experiments by a larger capillary connected to a humidifier controlled by Humisys software and facing the open edge of the sample capillary.

Infrared Microscopy. The water contents in the samples were determined with infrared spectroscopy on a Hyperion IR-microscope with a MCT detector with a resolution of 4 cm^{-1} in the range 900−8000 cm^{-1}. Data was collected in a line from the edge to the interior of the capillary with a step size of 25 μm and spatial resolution of 25 × 25 μm. Images were acquired at a magnification of 15×. The integral of the peak of the water OH bend−stretch at 4800−5300 cm^{-1} was used to determine the water content of the sample.[64] A calibration curve of octylglucoside−water solution at concentrations 0, 9, 20, 34, 43, and 50 wt % OG was used. The humidity was controlled by N_2 gas passed through 3 bubblers containing saturated salt solutions.

Raman Microscopy. Raman measurements were made on a LabRAM HR Evolution, Horiba, confocal Raman microscope with a green laser at 532 nm in the region between 1200 and 1800 cm^{-1}. Acquisition was set to 10 s with an accumulation of 10 at a magnification of 100×. The laser filter was set to 25% and 1200 gr/mm grafting. Measurements were made at a height of 50 μm down from the top of the film in lines from the air−liquid interface toward the dispersion reservoir in steps between 10 and 20 μm.

DOI: 10.1021/acscentsci.8b00362
ACS Cent. Sci. 2018, 4, 1315−1325

Cholesterol Concentration. The cholesterol concentration of the clinical lung surfactant extract Curosurf was determined by spectrophotometry after oxidation by cholesterol oxidase to 4-cholesten-3-one where hydrogen peroxide is a byproduct. The hydrogen peroxide is reacted with 4-aminophenon and phenol to form a color, which can be measured at 505 and 700 nm. Cholesterol esters are hydrolyzed to free cholesterol by cholesterol esterase. The analysis was performed by the clinical chemistry department at the Lund University Hospital.

■ ASSOCIATED CONTENT

Supporting Information

The Supporting Information is available free of charge on the ACS Publications website at DOI: 10.1021/acscentsci.8b00362.

1D and 2D SAXS spectra and peak assignment of phases, microscopy images, Raman measurements, water gradients determined by IR, and lamellar repeat distances (PDF)

■ AUTHOR INFORMATION

Corresponding Author

*E-mail: kevin.roger@ensiacet.fr.

ORCID

Kevin Roger: 0000-0001-7914-0951

Author Contributions

J.M.A., E.S., K.R., and M.L. designed the research. J.M.A. performed IR microscopy, polarized light microscopy, and SAXS/WAXS (bulk) experiments. J.M.A., K.R., and E.S. performed cSAXS experiments. J.M.A., K.R., and E.S. analyzed the experimental data. J.M.A., E.S., K.R., and M.L. interpreted the data. J.M.A., E.S., K.R., and M.L. wrote the paper.

Notes

The authors declare no competing financial interest.

Safety statement: no unexpected or unusually high safety hazards were encountered.

■ ACKNOWLEDGMENTS

The Swedish Foundation for Strategic Research and the Swedish Research Council (VR) is gratefully acknowledged for financial support (E.S.). Agence Nationale de la Recherche is acknowledged for financial support through Grant ANR-17-CE-09-0004-01 COATING (K.R.). The authors thank the Paul Scherrer Institute, Switzerland, for access to the beamline and Marianne Liebi for her assistance during the beam time. Per Persson and César Nicolás Cuevas are gratefully acknowledged for lending the IR microscope to us and help during the IR experiments. The Knut and Alice Wallenberg Foundation and the Faculty of Science, Lund University, are also acknowledged for the funding of the IR laboratory. We are also grateful to Irene Rodriguez Meizoso and Marta Espina Palanco for help with the Raman experiments and analysis. The Knut and Alice Wallenberg Foundation is also acknowledged for funding of the SAXS/WAXS instrument used for the bulk studies.

■ REFERENCES

(1) Daniels, C.; Orgeig, S. Pulmonary Surfactant: The Key to the Evolution of Air Breathing. *Physiology* **2003**, *18*, 151−157.

(2) Goerke, J. Lung Surfactant. *Biochim. Biophys. Acta, Rev. Biomembr.* **1974**, *344*, 241−261.

(3) Zuo, Y.; Veldhuizen, R.; Neumann, A.; Petersen, N.; Possmayer, F. Current Perspectives in Pulmonary Surfactant - Inhibition, Enhancement and Evaluation. *Biochim. Biophys. Acta, Biomembr.* **2008**, *1778*, 1947−1977.

(4) Fujiwara, T.; Maeta, H.; Chida, S.; Morita, T.; Watabe, T.; Abe, Y. Artificial Surfactant Therapy in Hyaline-Membrane Disease. *Lancet* **1980**, *315*, 55−59.

(5) Soll, R.; Blanco, F. Natural Surfactant Extract Versus Synthetic Surfactant for Neonatal Respiratory Distress Syndrome. *CDSR* **2001**, *2*, 144.

(6) Mussavi, M.; Mirnia, K.; Asadollahi, K. Comparison of the Efficacy of Three Natural Surfactants (Curosurf, Survanta, and Alveofact) in the Treatment of Respiratory Distress Syndrome Among Neonates: A Randomized Controlled Trial. *Iranian Journal of Pediatrics* **2016**, *26*, e5743.

(7) Obladen, M. History of Surfactant up to 1980. *Neonatology* **2005**, *87*, 308−316.

(8) Halliday, H. Overview of Clinical Trials Comparing Natural and Synthetic Surfactants. *Neonatology* **2004**, *67*, 32−47.

(9) Clark, R.; Auten, R.; Peabody, J. A Comparison of the Outcomes of Neonates Treated with Two Different Natural Surfactants. *J. Pediatr.* **2001**, *139*, 828−831.

(10) Rutkowska, M.; Hozejowski, R.; Helwich, E.; Borszewska-Kornacka, M.; Gadzinowski, J. Severe Bronchopulmonary Dysplasia - Incidence and Predictive Factors in a Prospective, Multicenter Study in Very Preterm Infants With Respiratory Distress Syndrome. *J. Matern.-Fetal Neonat. Med.* **2018**, *15*, 1−7.

(11) McIntyre, R.; Pulido, E.; Bensard, D.; Shames, B.; Abraham, E. Thirty Years of Clinical Trials in Acute Respiratory Distress Syndrome. *Crit. Care Med.* **2000**, *28*, 3314−3331.

(12) Dushianthan, A.; Cusack, R.; Goss, V.; Postle, A.; Grocott, M. Clinical Review: Exogenous Surfactant Therapy for Acute Lung Injury/Acute Respiratory Distress Syndrome - Where Do We Go From Here? *Critical Care* **2012**, *16*, 238.

(13) Casals, C.; Canadas, O. Role of Lipid Ordered Disordered Phase Coexistence in Pulmonary Surfactant Function. *Biochim. Biophys. Acta, Biomembr.* **2012**, *1818*, 2550−2562.

(14) Bernhard, W.; Mottaghian, J.; Gebert, A.; Rau, G.; von der Hardt, H.; Poets, C. Commercial Versus Native Surfactants, Surface Activity, Molecular Components, and the Effect of Calcium. *Am. J. Respir. Crit. Care Med.* **2000**, *162*, 1524−1533.

(15) Rüdiger, M.; Tölle, A.; Meier, W.; Rüstow, B. Naturally Derived Commercial Surfactants Differ in Composition of Surfactant Lipids and in Surface Viscosity. *Am. J. Physiol Lung Cell Mol. Physiol* **2005**, *288*, L379−L383.

(16) Lalchev, Z.; Todorov, R.; Exerowa, D. Thin Liquid Films as a Model to Study Surfactant Layers on the Alveolar Surface. *Curr. Opin. Colloid Interface Sci.* **2008**, *13*, 183−193.

(17) Pérez-Gil, J.; Keough, K. Interfacial Properties of Surfactant Proteins. *Biochim. Biophys. Acta, Mol. Basis Dis.* **1998**, *1408*, 203−217.

(18) Notter, R.; Tabak, S.; Mavis, R. Surface Properties of Binary Mixtures of Some Pulmonary Surfactant Components. *Journal of lipid research* **1980**, *21*, 10−22.

(19) Schürch, S. Surface Tension at Low Lung Volumes: Dependence on Time and Alveolar Size. *Respir. Physiol.* **1982**, *48*, 339−355.

(20) Notter, R. Pulmonary Surfactant: A Surface Chemistry Viewpoint. *Ann. Biomed. Eng.* **1975**, *3*, 119−159.

(21) Schürch, S.; Qanbar, R.; Bachofen, H.; Possmayer, F. The Surface-Associated Surfactant Reservoir in the Alveolar Lining. *Neonatology* **2004**, *67*, 61−76.

(22) Perez-Gil, J. Structure of Pulmonary Surfactant Membranes and Films: The Role of Proteins and Lipid-Protein Interactions. *Biochim. Biophys. Acta, Biomembr.* **2008**, *1778*, 1676−1695.

(23) Follows, D.; Tiberg, F.; Thomas, R.; Larsson, M. Multilayers at the Surface of Solution of Exogenous Lung Surfactant: Direct

DOI: 10.1021/acscentsci.8b00362
ACS Cent. Sci. 2018, 4, 1315−1325

Observation by Neutron Reflection. *Biochim. Biophys. Acta, Biomembr.* **2007**, *1768*, 228−235.
(24) Larsson, M.; Larsson, K.; Wollmer, P. The Alveolar Surface is Lined by a Coherent Liquid-Crystalline Phase. *Prog. Colloid Polym. Sci.* **2002**, *120*, 28−34.
(25) Kashchiev, D.; Exerowa, D. Structure and Surface Energy of the Surfactant Layer on the Alveolar Surface. *Eur. Biophys. J.* **2001**, *30*, 34−41.
(26) Å berg, C.; Sparr, E.; Larsson, M.; Wennerström, H. A Theoretical Study of Diffusional Transport Over the Alveolar Surfactant Layer. *J. R. Soc., Interface* **2010**, *7*, 1403−1410.
(27) Elias, P.; Friend, D. The Permeability Barrier in Mammalian Epidermis. *J. Cell Biol.* **1975**, *65*, 180−191.
(28) Butovich, I.; Millar, T.; Ham, B. Understanding and Analyzing Meibomian Lipids-A Review. *Curr. Eye Res.* **2008**, *33*, 405−420.
(29) Déry, R. The Evolution of Heat and Moisture in the Respiratory Tract During Anaesthesia with a Non-Rebreathing System. *Can. Anaesth. Soc. J.* **1973**, *20*, 296−309.
(30) Christie, R. V.; Loomis, A. L. The Pressure of Aqueous Vapour in the Alveolar Air. *J. Physiol.* **1932**, *77*, 35−48.
(31) Zuo, Y. Y.; Gitiafroz, R.; Acosta, E.; Policova, Z.; Cox, P. N.; Hair, M. L.; Neumann, A. W. Effect of Humidity on the Adsorption Kinetics of Lung Surfactant at Air-Water Interfaces. *Langmuir* **2005**, *21*, 10593−10601.
(32) Zuo, Y. Y.; Acosta, E.; Policova, Z.; Cox, P. N.; Hair, M. L.; Neumann, A. W. Effect of Humidity on the Stability of Lung Surfactant Films Adsorbed at Air-Water Interfaces. *Biochim. Biophys. Acta, Biomembr.* **2006**, *1758*, 1609−1620.
(33) Evans, D. F.; Wennerstöm, H. *The Colloidal Domain Where Physics, Chemistry, Biology and Technology Meet*, 2nd ed.; Wiley-VCH: Danvers, USA, 1999; Chapter 1.
(34) Markova, N.; Sparr, E.; Wadsö, L.; Wennerström, H. A Calorimetric Study of Phospholipid Hydration. Simultaneous Monitoring of Enthalpy and Free Energy. *J. Phys. Chem. B* **2000**, *104*, 8053−8060.
(35) Rand, R.; Parsegian, V. Hydration Forces Between Phospholipid Bilayers. *Biochim. Biophys. Acta, Rev. Biomembr.* **1989**, *988*, 351−376.
(36) Roger, K.; Liebe, M.; Heimdal, J.; Pham, Q.; Sparr, E. Controlling Water Evaporation Through Self-Assembly. *Proc. Natl. Acad. Sci. U. S. A.* **2016**, *113*, 10275−10280.
(37) Andersson, J.; Grey, C.; Larsson, M.; Ferreira, T.; Sparr, E. The Effect of Cholesterol on the Molecular Structure and Transitions in a Clinical Grade Lung Surfactant Extract. *Proc. Natl. Acad. Sci. U. S. A.* **2017**, *114*, E3592−E3601.
(38) Kim, K.; Choi, S.; Zell, Z.; Squires, T.; Zasadzinski, J. Effect of Cholesterol Nanodomains on Monolayer Morphology and Dynamics. *Proc. Natl. Acad. Sci. U. S. A.* **2013**, *110*, E3054−E3060.
(39) Bernardino de la Serna, J.; Pérez-Gil, J.; Simonsen, A.; Bagatolli, L. Cholesterol Rules: Diract Observations of the Coexistence of Two Fluid Phases in Native Pulmonary Surfactant Membranes at Physiological Temperatures. *J. Biol. Chem.* **2004**, *279*, 40715−40722.
(40) Al-Saiedy, M.; Gunasekara, L.; Green, F.; Pratt, R.; Chiu, A.; Yang, A.; Dennis, J.; Pieron, C.; Bjornson, C.; Winston, B.; Amrein, M. Surfactant Dysfunction in ARDS and Bronchiolitis is Repaired with Cyclodextrins. *Mil. Med.* **2018**, *183*, 207−214.
(41) Roger, K.; Sparr, E.; Wennerström, H. Evaporation, Diffusion and Self-Assembly at Drying Interfaces. *Phys. Chem. Chem. Phys.* **2018**, *20*, 10430−10438.
(42) Bastacky, J.; Lee, C. Y.; Goerke, J.; Koushafar, H.; Yager, D.; Kenaga, L.; Speed, T. P.; Chen, Y.; Clements, J. A. Alveolar Lining Layer is Thin and Continuous: Low-Temperature Scanning Electron Microscopy of Rat Lung. *J. Appl. Physiol.* **1995**, *79*, 1615−1628.
(43) Hall, J. *Guyton and Hall Textbook of Medical Physiology*, 13th ed.; Elsevier: Philadelphia, 2015.
(44) Marsh, D. *Handbook of Lipid Bilayers*; CRC Press: Boca Raton, FL, 1990; Chapter 2.
(45) Ulminus, J.; Wennerström, H.; Lindblom, G.; Arvidson, G. Deuteron Nuclear Magnetic Resonance Studies of Phase Equilibria in a Lecithin-Water System. *Biochemistry* **1977**, *16*, 5742−5745.
(46) Gulik-Krzywicki, T.; Rivas, E.; Luzzati, V. Structure et Polymorphisme des Lipides: Étude par Diffraction des Rayons X du Système Formé de Lipides de Mitochondries de Coeur de Boeuf et d'Eau. *J. Mol. Biol.* **1967**, *27*, 303−322.
(47) Ranck, J. L.; Zaccaï, G.; Luzzati, V. The Structure of a Lipid-Water Lamellar Phase Containing Two Types of Lipid Monolayers. An X-ray and Neutron Scattering Study. *J. Appl. Crystallogr.* **1980**, *13*, 505−512.
(48) Larsson, M.; Haitsma, J.; Lachmann, B.; Larsson, K.; Nylander, T.; Wollmer, P. Enhanced Efficacy of Porcine Lung Surfactant Extract by Utilization of its Aqueous Swelling Dynamics. *Clin. Physiol. Funct. Imaging* **2002**, *22*, 39−48.
(49) Gulik, A.; Tchoreloff, P.; Proust, J. A Conformation Transition of Lung Surfactant Lipids Probably Involved in Respiration. *Biophys. J.* **1994**, *67*, 1107−1112.
(50) Kumar, K.; Chavarha, M.; Loney, R. W.; Weiss, T. M.; Rananavare, S. B.; Hall, S. B. The L Phase of Pulmonary Surfactant. *Langmuir* **2018**, *34*, 6601−6611.
(51) Silva, T.; Claro, B.; Silva, B. F. B.; Vale, N.; Gomes, P.; Gomes, M. S.; Funari, S. S.; Teixeira, J.; Uhríková, D.; Bastos, M. Unravelling a Mechanism of Action for a Cecropin A-Melittin Hybrid Antimicrobial Peptide: The Induced Formation of Multilamellar Lipid Stacks. *Langmuir* **2018**, *34*, 2158−2170.
(52) Bernardino de la Serna, J.; Vargas, R.; Picardi, V.; Cruz, A.; Arranz, R.; Valpuesta, J. M.; Mateu, L.; Pérez-Gil, J. Segregated Ordered Lipid Phases and Protein-Promoted Membrane Cohesivity are Required for Pulmonary Surfactant Films to Stabilize and Protect the Respiratory Surface. *Faraday Discuss.* **2013**, *161*, 535−548.
(53) Å berg, C.; Sparr, E.; Wennerström, H. Lipid Phase Behaviour Under Steady State Conditions. *Faraday Discuss.* **2013**, *161*, 151−166.
(54) Lindblom, G.; Orädd, G. Lipid Lateral Diffusion and Membrane Heterogeneity. *Biochim. Biophys. Acta, Biomembr.* **2009**, *1788*, 234−244. Lipid Interactions, Domain Formation, and Lateral Structure of Membranes.
(55) Kõ iv, A.; Mustonen, P.; Kinnunen, K. Influence of Sphingosine on the Thermal Phase Behaviour of Neutral and Acidic Phospholipid Liposomes. *Chem. Phys. Lipids* **1993**, *66*, 123−134.
(56) Holopainen, J.; Lehtonen, J.; Kinnunen, P. Lipid Microdomains in Dimyristoylphosphatidylcholine-Ceramide Liposomes. *Chem. Phys. Lipids* **1997**, *88*, 1−13.
(57) Engelke, M.; Jessel, R.; Wiechmann, A.; Diehl, H. Effect of Inhalation Anaesthetics on the Phase Behaviour, Permeability and Order of Phosphatidylcholine Bilayers. *Biophys. Chem.* **1997**, *67*, 127−138.
(58) Mavromoustakos, T.; Theodoropoulou, E.; Papahatjis, D.; Kourouli, T.; Yang, D.-P.; Trumbore, M.; Makriyannis, A. Studies on the Thermotropic Effects of Cannabinoids on Phosphatidylcholine Bilayers Using Differential Scanning Calorimetry and Small Angle X-ray Diffraction. *Biochim. Biophys. Acta, Biomembr.* **1996**, *1281*, 235−244.
(59) Czamara, K.; Majzner, K.; Pacia, M. Z.; Kochan, K.; Kaczor, A.; Baranska, M. Raman Spectroscopy of Lipids: a Review. *J. Raman Spectrosc.* **2015**, *46*, 4−20.
(60) Schiller, J.; Hammerschmidt, S.; Wirtz, H.; Arnhold, J.; Arnold, K. Lipid Analysis of Bronchoalveolar Lavage Fluid (BAL) by MALDI-TOF Mass Spectrometry and 31P NMR Spectroscopy. *Chem. Phys. Lipids* **2001**, *112*, 67−79.
(61) Noack, G.; Berggren, P.; Curstedt, T.; Grossmann, G.; Herin, P.; Mortensson, W.; Nilsson, R.; Robertson, B. Severe Neonatal Respiratory Distress Syndrome Treated with the Isolated Phospholipid Fraction of Natural Surfactant. *Acta Paediatr.* **1987**, *76*, 697−705.
(62) Larsson, M.; Haitsma, J.; Lachmann, B.; Larsson, K.; Nylander, T.; Wollmer, P. Enhanced Efficacy of Porcine Lung Surfactant Extract by Utilization of its Aqueous Swelling Dynamics. *Clin. Physiol. Funct. Imaging* **2002**, *22*, 39−48.

DOI: 10.1021/acscentsci.8b00362
ACS Cent. Sci. 2018, 4, 1315−1325

(63) Larsson, M.; Larsson, K.; Nylander, T.; Wollmer, P. The Bilayer Melting Transition in Lung Surfactant Bilayers: the Role of Cholesterol. *Eur. Biophys. J.* **2003**, *31*, 633−636.
(64) Laughlin, R.; Lynch, M.; Marcott, C.; Munyon, R.; Marrer, A.; Kochvar, K. Phase Studies by Diffusive Interfacial Transport Using Near-Infrared Analysis for Water (DIT-NIR). *J. Phys. Chem. B* **2000**, *104*, 7354−7362.
(65) Sparr, E.; Wennerström, H. Interlamellar Forces and the Thermodynamic Characterization of Lamellar Phospholipid Systems. *Curr. Opin. Colloid Interface Sci.* **2011**, *16*, 561−567.
(66) Sodt, A. J.; Sandar, M. L.; Gawrisch, K.; Pastor, R. W.; Lyman, E. The Molecular Structure of the Liquid-Ordered Phase of Lipid Bilayers. *J. Am. Chem. Soc.* **2014**, *136*, 725−732.
(67) Sakurai, I.; Kawamura, Y. Growth Mechanism of Myelin Figures of Phosphatidylcholine. *Biochim. Biophys. Acta, Biomembr.* **1984**, *777*, 347−351.
(68) Mishima, K.; Yoshiyama, K. Growth Rate of Myelin Figures of Egg-Yolk Phosphatidylcholine. *Biochim. Biophys. Acta, Biomembr.* **1987**, *904*, 149−153.
(69) Sakurai, I.; Suzuki, T.; Sakurai, S. Cross-Sectional View of Myelin Figures. *Biochim. Biophys. Acta, Biomembr.* **1989**, *985*, 101−105.
(70) Buchanan, M.; Arrault, J.; Cates, M. Swelling and Dissolution of Lamellar Phases: Role of Bilayer Organization. *Langmuir* **1998**, *14*, 7371−7377.
(71) Bensimon, D. Stability of Viscous Fingering. *Phys. Rev. A: At., Mol., Opt. Phys.* **1986**, *33*, 1302−1308.
(72) Tsafrir, I.; Guedeau-Boudeville, M.; Kandel, D.; Stavans, J. Coiling Instability of Multilamellar Membrane Tubes with Anchored Polymers. *Phys. Rev. E: Stat. Phys., Plasmas, Fluids, Relat. Interdiscip. Top.* **2001**, *63*, 031603.
(73) Tsafrir, I.; Caspi, Y.; Guedeau-Boudeville, M.; Arzi, T.; Stavans, J. Budding and Tubulation in Highly Oblate Vesicles by Anchored Amphiphilic Molecules. *Phys. Rev. Lett.* **2003**, *91*, 138102.
(74) Inaba, T.; Kishimoto, T.; Murate, M.; Tajima, T.; Sakai, S.; Abe, M.; Marino, A.; Tomishige, N.; Ishitsuka, R.; Ikea, Y.; Takeoka, S.; Kobayashi, T. Phospholipase C1 Induces Membrane Tubulation and is Involved in Caveolae Formation. *Proc. Natl. Acad. Sci. U. S. A.* **2016**, *113*, 7834−7839.
(75) Parra, E.; Kinoshita, K.; Needham, D. Micropipette Technique Study of Natural and Synthetic Lung Surfactants at the Air-Water Interface: Presence of a SP-B Analog Peptide Promotes Membrane Aggregation, Formation of Tightly Stacked Lamellae, and Growth of Myelin Figures. *Langmuir* **2016**, *32*, 10570−10581.
(76) Sparr, E.; Hallin, L.; Markova, N.; Wennerström, H. Phospholipid-Cholesterol Bilayers under Osmotic Stress. *Biophys. J.* **2002**, *83*, 2015−2025.

DOI: 10.1021/acscentsci.8b00362
ACS Cent. Sci. 2018, 4, 1315−1325